Environmental Science & Technology

pubs.acs.org/est

Article

Global Spatiotemporal Variation and Death Burden of Compound Heatwave and Ozone Pollution Events

Ruijun Xu, Yuxin Bi, Xiaohong Jia, Yi Zheng, Nongping Feng, Sirong Wang, Lu Luo, Ziquan Lv, Suli Huang, Xue-Yan Zheng, Hong Sun, Gongbo Chen, Jing Wei,* and Yuewei Liu*

Cite This: *Environ. Sci. Technol.* 2026, 60, 8404−8414

Read Online

ACCESS | Metrics & More | Article Recommendations | Supporting Information

ABSTRACT: Heatwaves frequently coincided with ozone to form one of the most imminent health threats under global climate change. Identifying hotspots of compound heatwave and ozone pollution events (CHOEs) has crucial significance in developing targeted mitigation strategies, which is largely unknown. We therefore performed the comprehensive global and regional analyses on the spatiotemporal variation and death burden of CHOEs during 2000−2021. In addition to CHOE exposure, we estimated its population exposure through multiplying the exposure by total population. We observed that the frequency, duration, and intensity of CHOEs and their population exposures significantly increased in most midlatitudes, particularly in the Middle East and North Africa and South Asia. The population exposures increased at an accelerating pace and were mainly driven by the CHOE itself. We estimated that the death burden of CHOEs increased over time especially in the Middle East and North Africa, with a population attributable fraction of 0.99% in 2000 to 2.01% in 2021. Our findings add novel evidence that CHOEs markedly increased and posed substantial death burdens both regionally and globally in the past two decades. This evidence highlights urgent needs to develop regional targeted mitigation and adaptation actions to reduce health risks due to CHOEs, particularly in hotspots.

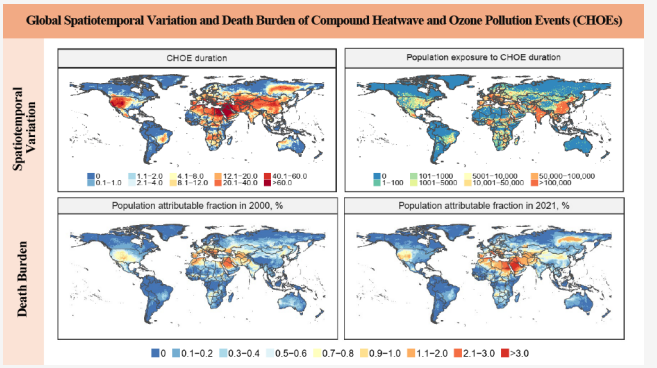

KEYWORDS: *compound heatwave and ozone pollution event, population exposure, spatiotemporal variation, death burden*

1. INTRODUCTION

Heatwave is defined as a prolonged period with extremely high temperatures and has been recognized as the most widespread weather event globally.[1,2] It was estimated that heatwaves accounted for more than 11% of all disaster deaths during 2000−2019 (about 0.15 million for 20 years; sourced from the Emergency Events Database) and were projected to cumulatively claim 1.6 million lives from 2023 to 2050 worldwide (sourced from the World Economic Forum).[3,4] In addition to direct health impacts, heatwaves (i.e., extreme temperatures) can accelerate atmospheric photochemical reaction and significantly increase the concentration of ground-level ozone (O_3), which is projected to increase in the future.[5,6] As a major greenhouse gas, ground-level O_3 can, in turn, amplify heatwaves through longwave radiative trapping and the deepening of isopycnals.[7] These reactions frequently make heatwaves and O_3 coincide to form compound heatwave and ozone pollution events (CHOEs).[8,9] To date, sporadic regional studies and one global study have identified certain vulnerable regions of CHOEs;[10−12] however, due to the limited coverage of regional studies and the coarse spatial resolution (130 km × 200 km) of the worldwide study, the global spatiotemporal variation of CHOEs is yet to be meticulously investigated, which hinders the distinction of potential exposure hotspots across the globe.

Emerging epidemiological studies have demonstrated that combined exposure to heatwaves and O_3 pollution can induce substantially greater effects on human health compared with the sum of their individual effects.[13−15] In our recent study in China, we provided novel and compelling evidence that the association of exposure to CHOEs with cardiovascular mortality was 1.6- to 3.2-folds higher than that in individual exposure to heatwaves or O_3 pollution.[15] A more recent study verified our results and further revealed that heatwaves and O_3 pollution can interact synergistically to trigger both nonaccidental and respiratory mortality.[14] These findings consistently suggest that CHOE is an imminent health threat

Received: December 5, 2025
Revised: February 24, 2026
Accepted: February 26, 2026
Published: March 9, 2026

under enhanced global climate change and may impose substantial death burdens on both individuals and the society.[16] It becomes essential and important to quantify the regional and global death burdens attributable to CHOEs to aid in the formulation of targeted mitigation and adaptation strategies; however, these death burdens still remain largely unknown.

To address these notable research gaps, we conducted global and regional analyses to (1) explore the spatiotemporal distribution and trend of CHOEs and their population exposures; (2) decompose the exposure, population, and their combined effects on population exposure changes; and (3) estimate the death burden of CHOEs, based on our generated global CHOE data sets from 2000 to 2021 with a high spatial resolution of 0.1 ° × 0.1 °.

2. METHODS

2.1. Data Collection

Gridded meteorological data were obtained from the land component of the fifth generation of European ReAnalysis (ERA5-Land) data set. The ERA5-Land data set is a derived data set of the land component from the European Centre for Medium-Range Weather Forecasts (ECMWF) and offers a long-term period since 1950 on an hourly scale and a high spatial resolution of 0.1 ° × 0.1 ° (approximately 9 km × 9 km).[17] As validated in previous studies, ERA5-Land data are highly accurate for temperature predictions.[18,19] The enhanced spatiotemporal resolution, comparably accurate predictions, and full spatiotemporal coverage make ERA5-Land an attractive data set for assessing variations in global and regional weather extremes. In this study, we collected global hourly 2 m air temperature (K) and 2 m dew point temperature (K) during 1961−2021 from the ERA5-Land data set and calculated daily mean air temperature and dew point temperature accordingly.

We obtained gridded ground-level daily maximum 8 h average (MDA8) O_3 concentration during 2000−2021 from our previously established GlobalHighAirPollutants (GHAP) data set (spatial resolution: 0.1 ° × 0.1 °; available at https://weijing-rs.github.io/product.html). The GHAP data set was produced with big data and artificial intelligence and has been well-known owing to its long-term, full-coverage, high-resolution, and high-quality characteristics. The global coefficient of determination (R^2) and root mean squared error (RMSE) for daily MDA8 O_3 estimates were 0.86 and 6.24 $\mu g/m^3$, respectively, and the R^2 and RMSE by monitoring-station density were, respectively, 0.82 and 6.95 $\mu g/m^3$,[20] indicating high agreement between the concentration prediction and its reference observations.

Annual gridded data for global population from 2000 to 2021 were derived from the LandScan Global Population Data set (https://landscan.ornl.gov/) with a spatial resolution of 30 arc-seconds (approximately 1 km × 1 km; Figure S1). The LandScan Global data set is currently the finest resolution publicly accessible population data set, which represents a global ambient population that can capture all potential activity space of people both in the day and night.[21] This data set is regarded as a comprehensive population distribution data set and has been commonly applied in many environmental and epidemiological researches.[22,23]

2.2. Definition of CHOEs

As a common apparent temperature indicator, the heat index (HI) is a measure of human perceived temperature and is estimated by the combination of air temperature and relative humidity. In comparison with using air temperature to define heatwaves, the application of HI can help provide more accurate exposure assessments.[24] In this study, we employed HI as the temperature metric and used the equations developed by Rothfusz in 1990 and adopted by the National Weather Service (NWS) to calculate HI based on the air temperature and dew point temperature data from the ERA5-Land data set (Supporting Information).[24]

To date, there has been no standard definition of heatwaves worldwide. We used the most common approach to define heatwaves with a combination of relative temperature threshold and duration.[25,26] As suggested by the World Meteorological Organization (WMO) Commission and previous studies, we used the period of 1961−1990 as the reference period and identified grid-specific heatwaves (spatial resolution: 0.1 ° × 0.1 °) when the daily HI reached or exceeded the 90th percentile of daily HIs during the reference period and lasted for at least 3 days (Figure S2).[27,28] According to the World Health Organization Air Quality Guidelines 2021 (WHO AQGs 2021), we defined grid-specific O_3 pollution events as the MDA8 O_3 concentration equal to or above 100 $\mu g/m^3$.[29] By this approach, each day in each grid will be classified as nonheatwave or heatwave day and non-O_3 pollution or O_3 pollution day according to its exposure to HI and O_3, respectively. For each grid, if a day is classified as both heatwave day and O_3 pollution day, this day will be defined as CHOE day. Finally, we generated a global gridded data set on CHOEs on a daily scale with a spatial resolution of 0.1 ° × 0.1 °.

We utilized three indicators, including frequency, duration, and intensity, to characterize CHOEs on a yearly scale. The frequency was defined as the number of CHOEs ($CHOE_f$, time), the duration was defined as the sum of all CHOE days ($CHOE_d$, day), while the intensity was defined as the weighted average value of the sum of standardized cumulative intensity across all CHOE days ($CHOE_i$). As proposed in previous studies, there was a significant difference in the health impacts between exposure to heatwaves and O_3 pollution.[14,15] To better capture their individual contributions to $CHOE_i$, we employed the risks of exposure to heatwaves and O_3 pollution to calculate the standardized and risk-weighted $CHOE_i$. $CHOE_i$ is a dimensionless indicator ranging from 0 to 1, with higher values indicating greater intensity. In this study, $CHOE_f$, $CHOE_d$, and $CHOE_i$ represent annual cumulative exposures to CHOE frequency, duration, and intensity in each grid during 2000−2021, respectively.

$$\text{CHOE frequency } (CHOE_f) = N$$

$$\text{CHOE duration } (CHOE_d) = \sum_{j=1}^{N} D_j$$

$$HI'_{jk} = \frac{(HI_{jk} - HI_0) - \min\limits_{1\le x\le CHOE_d}(HI_x - HI_0)}{\max\limits_{1\le x\le CHOE_d}(HI_x - HI_0) - \min\limits_{1\le x\le CHOE_d}(HI_x - HI_0)}$$

$$Ozone'_{jk} = \frac{(Ozone_{jk} - Ozone_0) - \min\limits_{1\le x\le CHOE_d}(Ozone_x - Ozone_0)}{\max\limits_{1\le x\le CHOE_d}(Ozone_x - Ozone_0) - \min\limits_{1\le x\le CHOE_d}(Ozone_x - Ozone_0)}$$

$$\text{CHOE intensity } (CHOE_i) = \frac{\beta_{HW} \times \sum_k^N \sum_j^{D_j} HI'_{jk} + \beta_{Ozone} \times \sum_k^N \sum_j^{D_j} Ozone'_{jk}}{\beta_{HW} + \beta_{Ozone}}$$

where N is the total number of CHOEs in each year; D_j is the total days of the jth CHOE; HI_0 is the 90th percentile of daily mean HI during 1961−1990; HI_{jk} is the mean HI in the kth day of the jth CHOE; $Ozone_0$ is the threshold of O_3 pollution events (i.e., 100 $\mu g/m^3$); $Ozone_{jk}$ is the O_3 concentration in the kth day of the jth CHOE; x is the xth CHOE day; HI'_{jk} is the standardized excess HI in the kth day of the jth CHOE; $Ozone'_{jk}$ is the standardized excess O_3 in the kth day of the jth CHOE; β_{HW}[31] and β_{Ozone}[31,32] represent the mortality risk estimates of exposure to heatwaves and O_3 pollution, which were collected from previous studies (Supporting Information).

To account for the variation of population distribution, we unified the spatial resolution of the LandScan Global data set as 0.1 ° × 0.1 ° and calculated the population exposure to CHOEs by multiplying each of the three indicators by the annual population for each grid cell

https://doi.org/10.1021/acs.est.5c17533
Environ. Sci. Technol. 2026, 60, 8404−8414

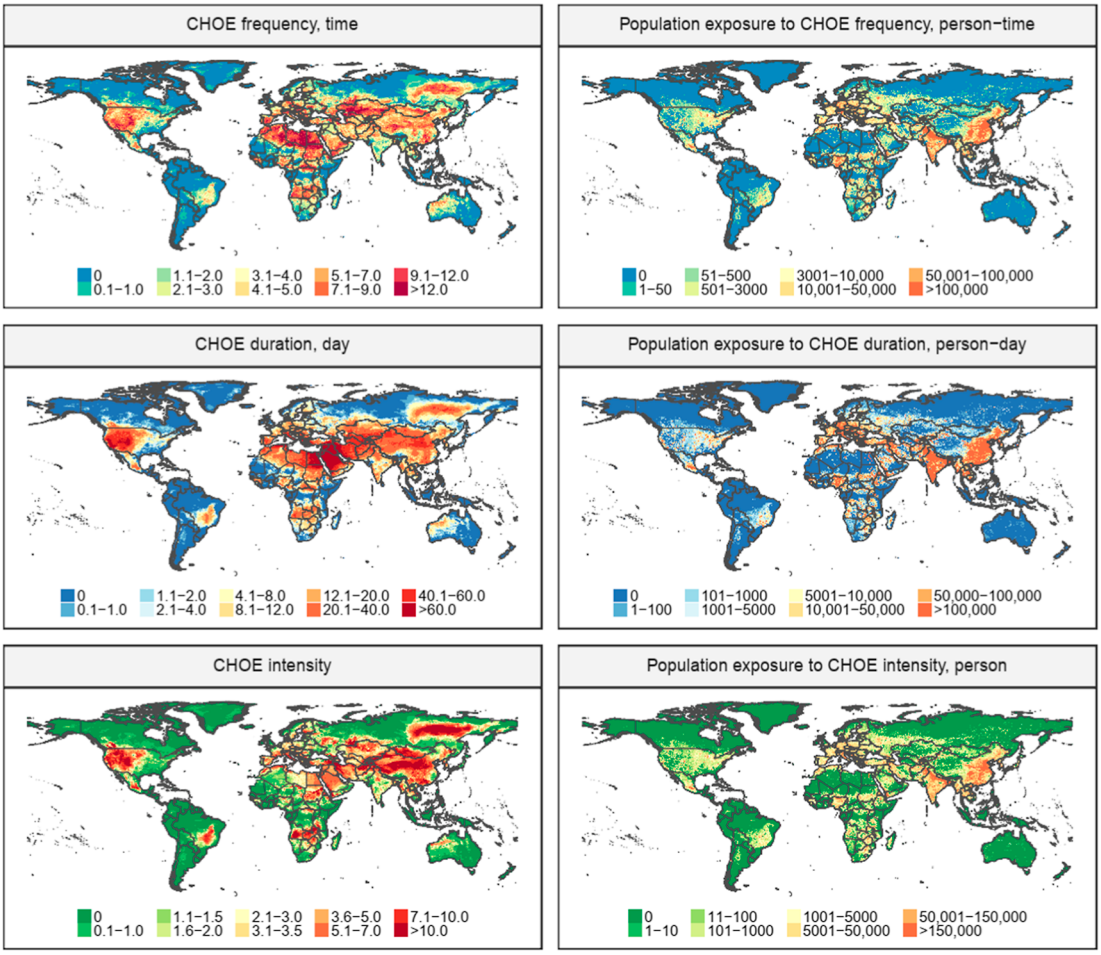

Figure 1. Spatial distribution of CHOEs and their population exposures in 2021. CHOEs, compound heatwave and ozone pollution events.

from 2000 to 2021, including population exposure to $CHOE_f$ (Pop-$CHOE_f$; person-time), population exposure to $CHOE_d$ (Pop-$CHOE_d$; person-day), and population exposure to $CHOE_i$ (Pop-$CHOE_i$; person). The Pop-$CHOE_f$, Pop-$CHOE_d$, and Pop-$CHOE_i$ represent population exposure to $CHOE_f$, $CHOE_d$, and $CHOE_i$, respectively.

2.3. Statistical Analysis

We first calculated the annual sum of $CHOE_f$, $CHOE_d$, and $CHOE_i$ and their corresponding population exposures at each grid from 2000 to 2021. To explore the spatiotemporal variation of CHOEs on a regional scale, we divided the world into different regions according to the latest World Bank income and regional group classification, including 218 countries/regions, four World Bank income groups (high-income, low-income, lower-middle-income, and upper-middle-income countries), and seven of eight World Bank regional groups (Latin America and Caribbean, Europe and Central Asia, South Asia, Sub-Saharan Africa, Middle East and North Africa, East Asia and Pacific, and North America; the Antarctica is excluded due to the lack of a native human population; Figure S3). We then calculated the mean values of the three CHOE indicators for each grid within the globe and each region.

The spatial autocorrelation of both CHOEs and the population exposures was tested using the Global Moran's I index.[33] Since this index can only measure the spatial pattern for the entire area, we also performed cluster and outlier analyses (i.e., Local Moran's I index) to explore any hotspot of CHOEs.[34] A negative Moran's I index indicates a tendency toward dispersion, a positive index represents a tendency toward clustering, while a zero index means that the occurrence is randomly distributed. The Moran's I index was statistically significant when a z score was less than -1.96 or more than 1.96 and the corresponding P value on a global or regional scale (or adjusted P value on a grid scale calculated by the false discovery rate [FDR] method) was lower than 0.05.[33−35] For cluster and outlier analyses, four different clusters were considered statistically significant, including high-high ($P < 0.05$, $I > 0$, and $z > 1.96$), high-low ($P < 0.05$, $I < 0$, and $z > 1.96$), low-high ($P < 0.05$, $I < 0$, and $z < -1.96$), and low-low ($P < 0.05$, $I > 0$, and $z < -1.96$) clusters. The high-high cluster indicates that the region and its adjacent regions are vulnerable zones of CHOEs with high values (i.e., hotspots), the high-low (or low-high) cluster represents that a high-valued (or low-valued) area surrounded by low-valued (or high-valued) neighbors, while the low-low cluster means that the region and its neighboring regions are cold spots with low values.

The temporal trends of CHOEs and population exposures from 2000 to 2021 were calculated through Sen's Kendall slope estimator, which is nonparametric and robust against measurement errors or outliers.[36,37] The Sen's Kendall slope estimator provides a confidence interval for the estimated spatiotemporal trend. A z score above 1.96 indicates a significant increasing trend, while a z-score less than -1.96 represents a significant decreasing trend. Temporal trend analyses were performed on a gridded, regional, and global level. A two-sided P value on a global or regional scale (or adjusted P value on a grid scale calculated by the FDR method) of less than 0.05 was considered to be statistically significant.

To explicitly examine the potential effect of exposure and population distribution on spatiotemporal changes in population exposure, we decomposed the population exposure changes into exposure, population, and their combined effect on both global and regional scales.[38,39] Specifically, the exposure effect reflected the impact of changes in $CHOE_f$ (or $CHOE_d$, or $CHOE_i$; i.e., the contribution of changes in CHOE metrics to population exposure changes), the population effect represented the influence of variations

https://doi.org/10.1021/acs.est.5c17533
Environ. Sci. Technol. 2026, 60, 8404−8414

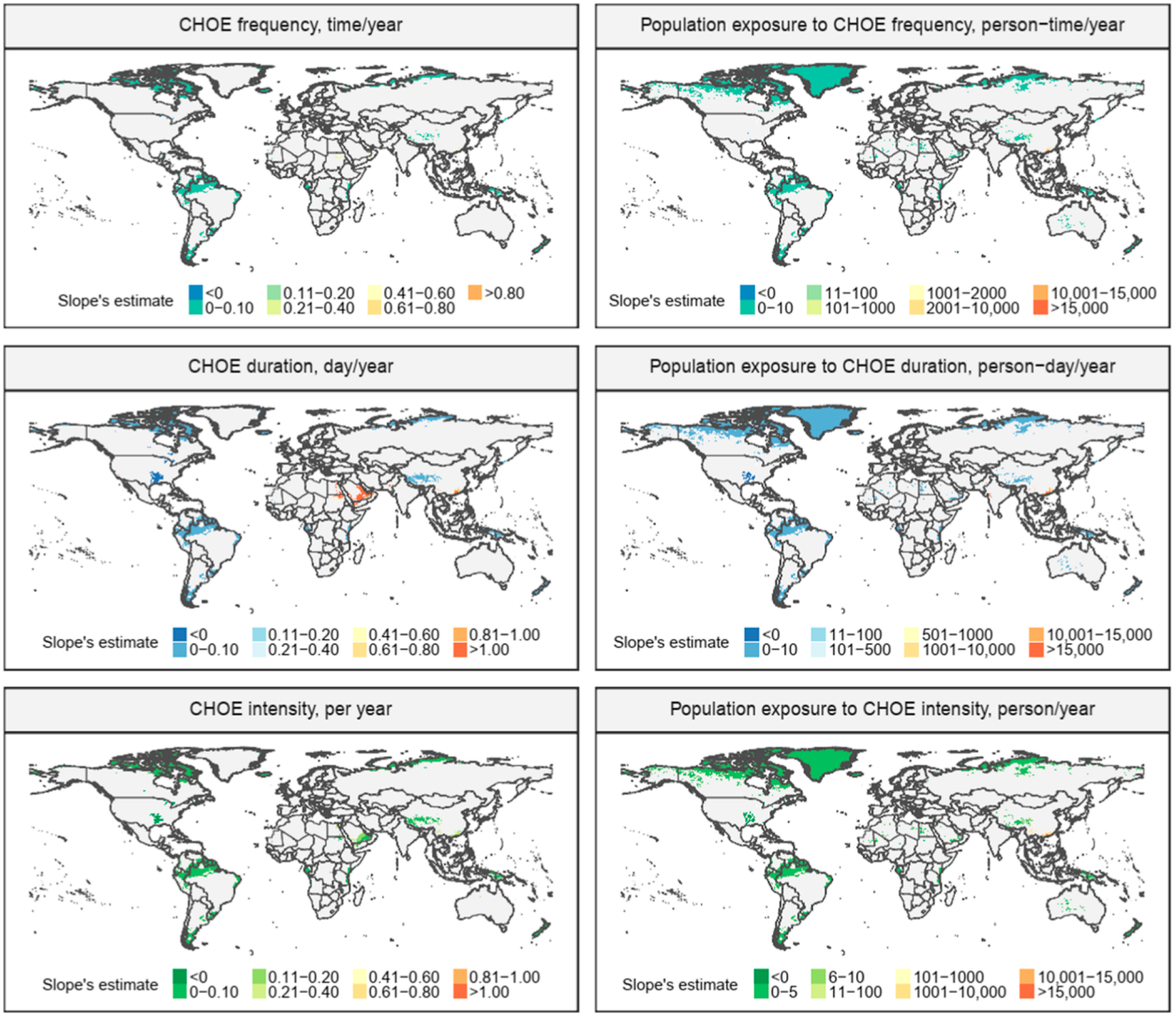

Figure 2. Spatial distribution of Slope's estimates of annual changes in CHOEs and their population exposures from 2000 to 2021. CHOEs, compound heatwave and ozone pollution events. The *P* value was adjusted by the false discovery rate method.

on both size and distribution of population, while the combined effect referred to the intertwined impact of changes in both exposure and population shifts. The decomposition of these three effects on population exposure changes was calculated using the following formula.

$$\Delta\text{Exposure}_j = \text{CHOEs}_{2000} \times \Delta\text{Population}_j + \text{Population}_{2000} \times \Delta\text{CHOEs}_j + \Delta\text{CHOEs}_j \times \Delta\text{Population}_j$$

where $\triangle\text{Exposure}_j$ represents changes of population exposure in year j using population exposure in 2000 as the reference; CHOEs_{2000} represents CHOEs (CHOE_f, CHOE_d, or CHOE_i) in 2000; $\triangle\text{Population}_j$ represents changes in population in year j compared with the population in 2000; Population_{2000} represents the population in 2000; and $\triangle\text{CHOEs}_j$ represents changes of CHOEs in year j compared with exposure in 2000.

Based on the estimated annual decompositions in population exposure changes mentioned above, we utilized linear regression models to explore the temporal trend for each decomposed effect from 2000 to 2021 across the globe and different regions. A negative β indicates a significant decreased trend and a positive β represents a significant increased trend, when the corresponding *P* value is less than 0.05.

We applied population attributable fraction (PAF) with and without being weighted by the total population to, respectively, quantify the death burden of CHOEs for each gird and region, using the following formulas.

$$\text{PAF}_{y,p} = \frac{\sum_{j=1}^{n}\left(1 - \frac{1}{e^{(\beta_{y,p}\times \text{CHOE}_{y,p,j})}}\right)}{n} \times 100\%$$

$$\text{PAF}_y = \frac{\sum_{p=1}^{P}(\text{Pop}_{y,p} \times \text{PAF}_{y,p})}{\sum_{p=1}^{P}\text{Pop}_{y,p}}$$

where $\text{PAF}_{y,p}$ represents the PAF in year y and in grid p; n represents the total days in year y; $\beta_{y,p}$ represents the risk estimate of the association between exposure to CHOEs and mortality in year y and in grid p, which was calculated based on risk estimates for heatwaves[30,40] and O_3 pollution[31,32,40] exposures reported in previous studies (Supporting Information); $\text{CHOE}_{y,p,j}$ represents whether day j was a CHOE day or not (yes = 1, no = 0) in year y and in grid p; PAF_y represents the population weighted PAF in one region in year y, in order to consider the potential impacts of population; P represents total number of grids in the region; and $\text{Pop}_{y,p}$ represents the total population in year y and in grid p. Linear regression models were used to explore temporal trends for the death burden on both global and regional scales.

https://doi.org/10.1021/acs.est.5c17533
Environ. Sci. Technol. 2026, 60, 8404−8414

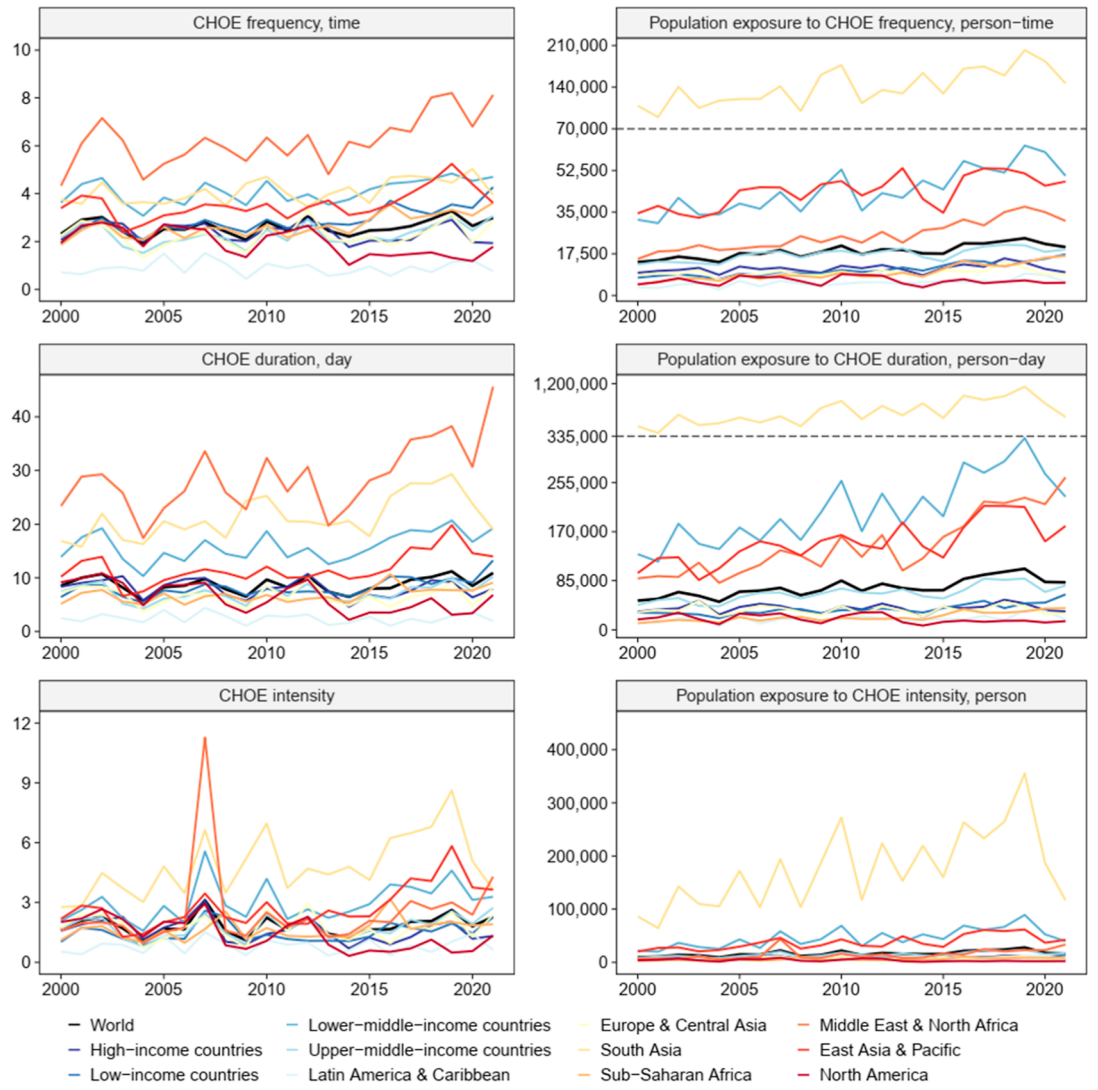

Figure 3. Temporal distribution of global and regional CHOEs and their population exposures from 2000 to 2021. CHOEs, compound heatwave and ozone pollution events.

Several sensitivity analyses were conducted to test the robustness of our results, including adjusting referent time for the temperature threshold of heatwaves from 1961−1990 to 1971−2000, quantifying $CHOE_i$ by averaging the sum of standardized intensities of heatwaves and O_3 pollution (Supporting Information), and changing the concentration threshold for O_3 pollution to 80 and 120 $\mu g/m^3$. All analyses were performed in R software (version 4.4.2), and a two-sided P value less than 0.05 was considered significant.

3. RESULTS

3.1. Global CHOEs and Their Population Exposures

In 2021, more $CHOE_f$, longer $CHOE_d$, and higher $CHOE_i$ mainly concentrated in midlatitudes. More population exposures were primarily observed in eastern China, India, and southern Europe (Figures 1 and S4−S10). The global average $CHOE_f$, $CHOE_d$, and $CHOE_i$ in 2021 was 3.0 times, 10.9 days, and 2.3, respectively, while the corresponding population exposure was 20,314.1 person-times, 82,028.3 person-days, and 16,208.4 persons, respectively (Tables S1−S6).

The Global Moran's I index of CHOEs in each year from 2000 to 2021 was significantly positive (ranging from 0.96 to 0.99, all $P < 0.001$), indicating that the global spatial distribution patterns of CHOEs were significantly clustered (Tables S7−S9). In the cluster and outlier analyses, only a cluster of high-high CHOEs was observed mainly in northern midlatitude regions. Similar spatial autocorrelation was detected for the population exposures, with slightly smaller Global Moran's I indexes ranging from 0.48 to 0.74 during the study period (Figures S11−S17).

The $CHOE_f$ has significant increasing trends in southeastern Asia, south China, southeastern Arabian Peninsula, and small areas of the North Africa and Sub-Saharan Africa; $CHOE_d$ and $CHOE_i$ demonstrated widespread and significant increasing trends during the study period and mainly concentrated over parts of southeastern Asia, south China, the Arabian Peninsula, North Africa, and Sub-Saharan Africa. For population exposure, significant increased trends were consistent in northeastern Asia, south China, South Asia, Middle East, North Africa, and Sub-Saharan Africa (Figure 2). On a global scale, three CHOE indicators demonstrated a slightly but insignificant increase during the study period (all Sen's slope values < 0.1, $P > 0.05$); instead, the temporal trend of population exposures was significantly positive, with a Sen's slope value of 378.1 person-times/year, 1973.5 person-days/

https://doi.org/10.1021/acs.est.5c17533
Environ. Sci. Technol. 2026, 60, 8404−8414

Table 1. Top 10 Countries or Regions in Temporal Trends of CHOEs and Their Population Exposures from 2000 to 2021[a]

Area	Frequency	Area	Duration	Area	Intensity
CHOEs					
Yemen	0.29[c]	Qatar	2.70[c]	Bahrain	0.48[c]
Hong Kong, China	0.27[c]	Bahrain	2.20[c]	Qatar	0.37[c]
Arab Republic of Egypt	0.23[b]	United Arab Emirates	2.08[c]	Tajikistan	0.34[c]
Macao, China	0.22[b]	Kuwait	1.75[b]	Kyrgyz Republic	0.33[c]
Sudan	0.21[b]	Saudi Arabia	1.67[c]	Hong Kong, China	0.26[c]
Lebanon	0.19[c]	Jordan	1.40[c]	Macao, China	0.26[c]
Oman	0.17[c]	West Bank and Gaza	1.33[b]	West Bank and Gaza	0.17[c]
Saudi Arabia	0.17[b]	Israel	1.30[b]	United Arab Emirates	0.17[c]
Eritrea	0.16[c]	Arab Republic of Egypt	1.24[b]	India	0.17[b]
Sierra Leone	0.15[b]	Tajikistan	1.15[c]	Zimbabwe	0.17[b]
Population exposures					
Macao, China	207,201.5[b]	Bahrain	675,170.5[c]	Macao, China	226,809.3[c]
Hong Kong, China	180,391.8[c]	Macao, China	550,412.5[b]	Hong Kong, China	127,123.9[c]
West Bank and Gaza	22,181.9[c]	Hong Kong, China	491,877.0[c]	Bahrain	123,074.4[c]
Bangladesh	18,628.9[c]	West Bank and Gaza	139,453.8[b]	Bangladesh	19,727.9[c]
Israel	14,925.5[b]	Qatar	93,050.9[c]	West Bank and Gaza	14,637.3[c]
Lebanon	14,713.1[c]	Israel	72,911.4[b]	Qatar	11,237.6[c]
Republic of Korea	8040.7[b]	Bangladesh	66,078.9[b]	India	10,732.8[c]
San Marino	5522.5[c]	Lebanon	47,294.9[c]	Republic of Korea	10,016.1[b]
Nigeria	4944.9[c]	India	33,159.7[b]	Israel	8983.3[b]
Qatar	4044.0[b]	Jordan	32,031.5[c]	Lebanon	6011.4[b]

[a]CHOEs, compound heatwave and ozone pollution events. The unit of slope' estimate of CHOE frequency, duration, and intensity was time/year, day/year, and per year, respectively, while the unit of slope' estimate of population exposure to CHOE frequency, duration, and intensity was person-time/year, person-day/year, and person/year, respectively. [b]$P < 0.05$. [c]$P < 0.001$.

year, and 499.7 persons/year for the Pop-$CHOE_f$, Pop-$CHOE_d$, and Pop-$CHOE_i$, respectively (Table S13).

3.2. Regional CHOEs and Their Population Exposures

3.2.1. Exposure in Four World Bank Income Groups. Among four World Bank income groups, the most serious CHOEs and population exposures in 2021 were observed in lower-middle-income countries, with the value of 4.7 times for $CHOE_f$, 19.2 days for $CHOE_d$, 3.3 for $CHOE_i$, 50,277.9 person-times for Pop-$CHOE_f$, 230,395.1 person-days for Pop-$CHOE_d$, and 39,795.0 persons for $CHOE_i$, respectively (Figure 3 and Tables S1−S6).

Significantly increasing trends of the three CHOE indicators were observed in low-income, lower-middle-income, and upper-middle-income countries, showing the fastest increasing trend in low-income countries for the $CHOE_f$ (Sen's slope value = 0.07 times/year) and $CHOE_d$ (0.13 days/year) and in lower-middle-income countries for the $CHOE_i$ (0.06 per year). For population exposure, the sharpest rising trends were observed in lower-middle-income countries, with the Sen's slope values of 1184.1 person-times/year, 7332.5 person-days/year, and 1856.1 persons/year for the Pop-$CHOE_f$, Pop-$CHOE_d$, and Pop-$CHOE_i$, respectively (Table S13).

3.2.2. Exposure in Seven World Bank Regional Groups. As shown in Figure 3, the most CHOEs among the different World Bank regional groups in 2021 were observed in the Middle East and North Africa, with the value of 8.1 times, 45.6 days, and 4.3 for $CHOE_f$, $CHOE_d$, and $CHOE_i$, respectively. For population exposures, most Pop-$CHOE_f$, Pop-$CHOE_d$, and Pop-$CHOE_i$ occurred in South Asia, with the values of 146,260.2 person-times, 623,836.5 person-days, and 116,853.0 persons, respectively (Tables S1−S6).

Among the seven World Bank regional groups, temporal trends in CHOEs continued to increase from 2000 to 2021 (Table S13). $CHOE_f$ and $CHOE_d$ increased with the sharpest trend in the Middle East and North Africa (Sen's slope value = 0.11 times/year and 0.52 days/year), while the most obvious increased trend in $CHOE_i$ occurred in the South Asia with a Sen's slope value of 0.13 per year. Although there was an overall uptrend in $CHOE_i$ in the Middle East and North Africa, year like 2007 stood out with particularly severe intensity. For population exposure, the sharpest uptrends were observed in the South Asia, with the Sen's slope value of 3322.3 person-times/year for Pop-$CHOE_f$, 26,869.4 person-days/year for Pop-$CHOE_d$, and 7096.5 persons/year for Pop-$CHOE_i$, respectively.

3.2.3. Exposure in 218 Countries/Regions. In 2021, the highest $CHOE_f$, longest $CHOE_d$, and greatest $CHOE_i$ among 218 countries/regions were 10.8 times in the Arab Republic of Egypt, 81.6 days in Kuwait, and 15.7 days in Bahrain, respectively. For population exposure, we observed the longest Pop-$CHOE_d$ in Bahrain (15,196,654.0 person-days), while the most Pop-$CHOE_f$ and highest Pop-$CHOE_i$ were both located in Macao, China (4,215,875.0 person-times and 5,156,507.6 persons; Table S10−S12).

During 2000−2021, the most obvious increasing trends of the $CHOE_f$, $CHOE_d$, and $CHOE_i$ among 218 countries/regions, respectively, appeared in Yemen, Qatar, and Bahrain, with the corresponding Sen's slope estimate of 0.29 times/year, 2.70 days/year, and 0.48 per year. We observed the largest temporal trends of the Pop-$CHOE_f$, Pop-$CHOE_d$, and Pop-$CHOE_i$ in Macao, China, Bahrain, and Macao, China, respectively (Sen's slope value: 207,201.5 person-times/year, 675,170.5 person-days/year, and 226,809.3 persons/year; Table 1 and Tables S14−S15).

https://doi.org/10.1021/acs.est.5c17533
Environ. Sci. Technol. 2026, 60, 8404−8414

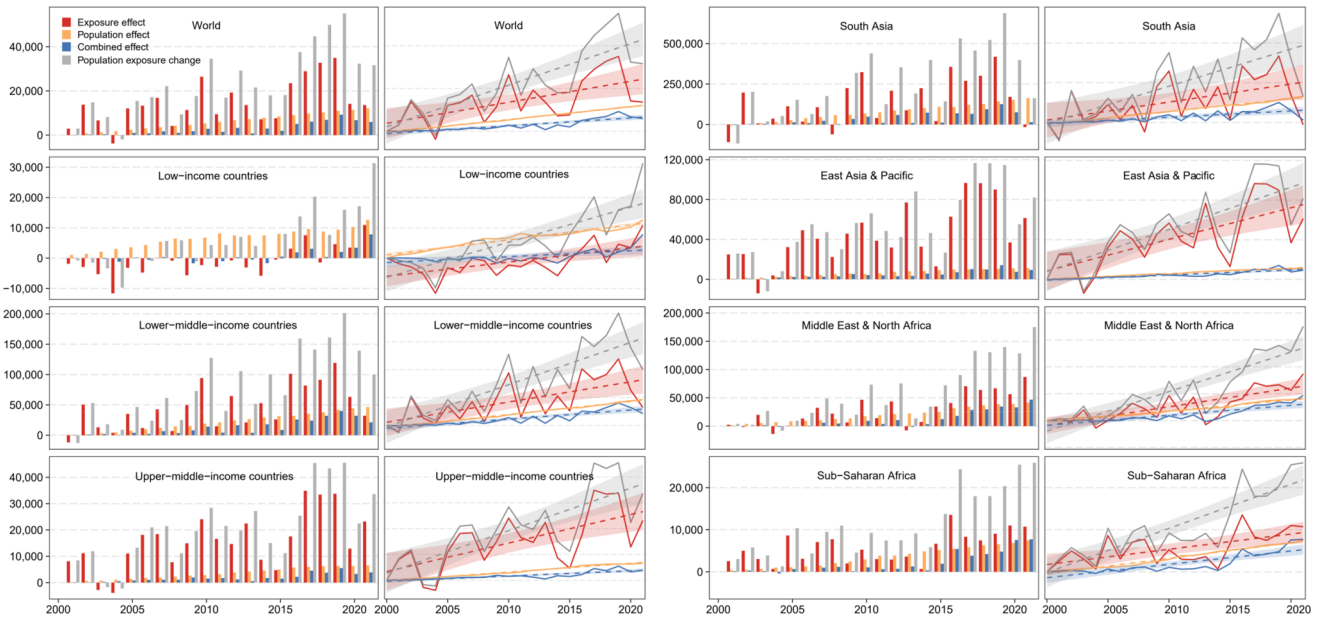

Figure 4. Decomposition of changes in population exposure to CHOE duration and their linear trends worldwide and in seven regions from 2000 to 2021. CHOE, compound heatwave and ozone pollution event.

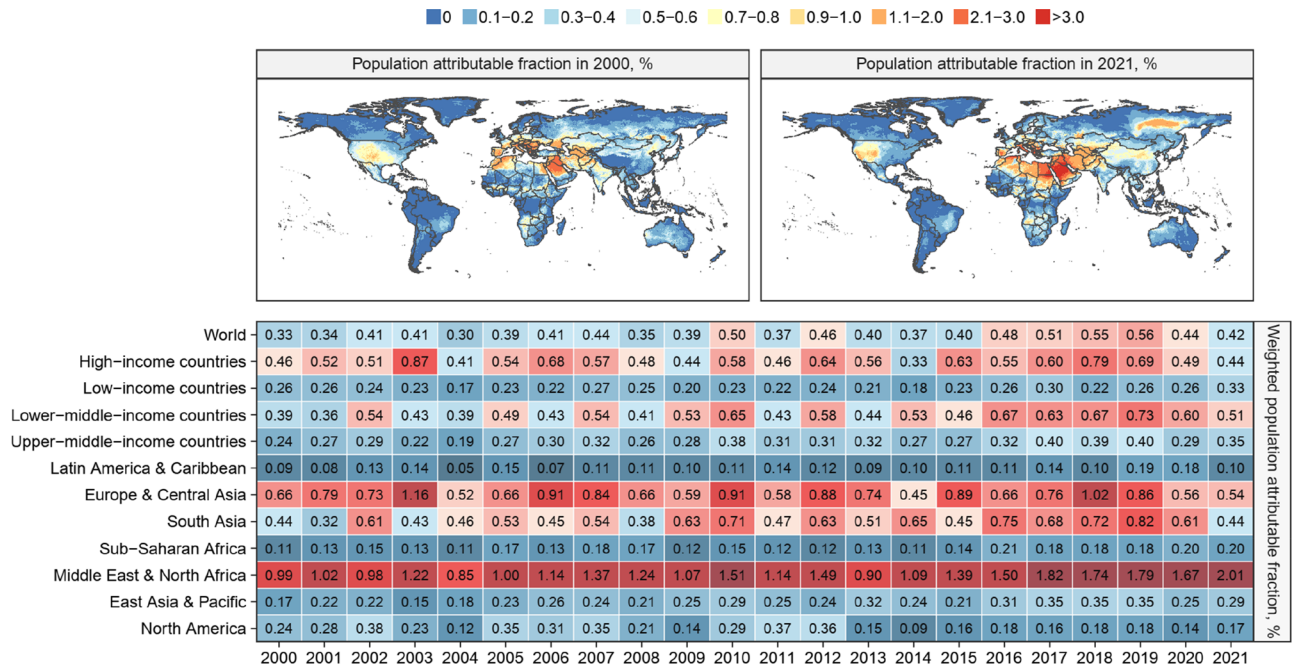

Figure 5. Population attributable fraction due to CHOEs from 2000 to 2021. CHOEs, compound heatwave and ozone pollution events.

3.3. Decomposition of Population Exposure Changes

Using the exposure and population data in 2000 as a reference, we observed that there was a significant increasing trend in the duration, frequency, and intensity of population exposure changes worldwide over the past two decades (Figure 4). In general, the global population exposure changes increased nonmonotonically from 2001 to 2021, with the corresponding annual rise averaged of 374.4 person-times, 1943.2 person-days, and 516.7 persons for the Pop-CHOE$_f$, Pop-CHOE$_d$, and Pop-CHOE$_i$, respectively ($P < 0.001$). Similar increasing trends were observed in all included World Bank incomes and regional groups (Table S16).

When decomposing population exposure changes into the exposure, population, and their interactions, we observed distinct impacts from each factor across the globe and different regions (Figures 4, Table S16 and S18−S21). On a global scale, the exposure effect contributed to most proportion and increase in population exposure changes of the Pop-CHOE$_f$ (proportion up to 88.0%; 161.2 person-times), Pop-CHOE$_d$ (98.1%; annual averaged rise of 981.6 person-days), and Pop-CHOE$_i$ (62.2%; 321.3 persons). Among different regions, the exposure effect generally accounted for the highest proportion in population exposure changes and showed the sharpest increased trend in annual changes (e.g., the population exposure change of Pop-CHOE$_f$ and its exposure effect in

https://doi.org/10.1021/acs.est.5c17533
Environ. Sci. Technol. 2026, 60, 8404−8414

the East Asia and Pacific were 437.8 person-times and 722.2 person-times, respectively, suggesting that 60.6% of population exposure change was attributable to exposure change), despite that the population effect contributed most to the population exposure changes in low-income countries, lower-middle-income countries, the South Asia, and Middle East and North Africa for the Pop-$CHOE_f$, and in the Sub-Saharan Africa for the Pop-$CHOE_i$.

3.4. Death Burden of CHOEs

As presented in Figure 5, the PAF of CHOEs in 2021 was higher in lower-middle-income countries (0.51%), the Europe and Central Asia (0.54%), and Middle East and North Africa (2.01%). Of them, trend analysis showed that the death burden significantly increased in lower-middle-income countries, upper-middle-income countries, the South Asia, Sub-Saharan Africa, Middle East and North Africa, and Europe and Central Asia, but significantly decreased in the North America ($P < 0.05$; Table S17). Among 218 countries/regions, the highest PAF in 2021 was, respectively, observed in Kuwait (3.21%; 95% CI: 3.02%, 3.36%), both showing a significant increasing trend from 2000 to 2021 ($P < 0.05$; Tables S18−S20).

Sensitivity analyses by adjusting the referent time for the temperature threshold of heatwaves from 1961−1990 to 1971−2000 (Figures S23−S27), quantifying $CHOE_i$ by averaging the sum of standardized intensities of heatwaves and O_3 pollution (Figures S28−S32), and changing the concentration threshold for O_3 pollution (Figures S33 and S34) all yielded similar results.

4. DISCUSSION

Based on multisource fine-resolution reanalysis products, we performed a comprehensive global and regional analysis of the spatiotemporal variation and death burden of CHOEs in the past two decades. We found that CHOEs displayed evident increasing trends and posed substantial death burdens during 2000−2021. Higher frequency, longer duration, and greater intensity of CHOEs and their population exposures distributed in midlatitude regions and significantly increased especially in the Middle East and North Africa and South Asia. The Pop-CHOEs acceleratingly increased and were mainly contributed by the occurrence of CHOEs. The death burden of CHOEs was considerable and showed an increasing trend over time, with the highest PAF of 0.99% in 2000 to 2.01% in 2021 in the Middle East and North Africa.

There were pronounced spatial heterogeneities and increasing trends in CHOEs across the globe. The results of Local Moran's I index revealed a cluster of high-high CHOEs in northern midlatitude regions (i.e., hotspots of CHOEs). Specifically, more frequent and intense CHOEs were distributed in midlatitudes, while the distribution of population exposures indicates a similar but clearer tendency in densely populated areas. This is in line with the patterns of population exposures reported in another study in 2022, which merely focused on the spatial distribution of $CHOE_d$ during 1995−2014.[10] Of note, the definition of O_3 pollution in this exiting study was at least two consecutive days with the MDA8 O_3 concentration exceeded the WHO AQGs 2021 threshold, which may lead to much lower estimates on global annual mean $CHOE_d$ (2.6 vs 8.7 days). Unlike a single event, CHOEs were formed by the coincidence of exposure to two single events. It should be noted that the quantile-based temperature threshold for heatwave captures local extremes (i.e., climate anomaly/extremeness), whereas the absolute threshold for O_3 pollution reflects health exceedances (i.e., risk identification). The variation in the definition of heatwaves or O_3 pollution was likely to impact the quantification of CHOEs and serves as the main reason for the heterogeneity in findings across studies. Given that growing evidence suggests that exposure to heatwaves and O_3 pollution can interact to cause human health hazards, our findings not only identify vulnerable CHOE regions but also highlight the urgent needs to further elucidate the health impacts of CHOEs in these hotspots.[13−15,41]

In our regional analyses in different income groups, we revealed thought-provoking evidence that the population living in the low- and lower-middle-income countries were faced with substantial exposures and death burdens of CHOEs. More importantly, these regions displayed the greatest increase in trend magnitudes of CHOEs at the same time. This pattern indicates that people in these countries have suffered from the most severe CHOEs, and they will experience more events under the current exposure scenario in the future. It should be noted that the majority of people in low- and lower-middle-income countries lack awareness, adaptation measures, and resources to address climate change; they tend to suffer from elevated surface O_3 concentrations due to the large increase in future precursors and more enhancive heatwaves under global climate warming, which will amplify inequalities in population exposures across different income groups.[42,43] Therefore, we advocate that certain measures are urgently needed to help countries with lower incomes to better proactively reduce these inequalities and cope with climate change in the future, including improvements in CHOE early warning systems, international organization assistance for adaptation projects, and knowledge sharing, as well as policy interventions.[28,44,45]

Our regional analyses among seven World Bank regional groups demonstrated that the South Asia, Middle East and North Africa, and East Asia and Pacific were vulnerable hotspots to CHOEs. Among these, the Middle East and North Africa were exposed to the most and significant increased CHOEs. Additionally, taking population pattern into consideration, we found that South Asia has become the most severe hotspot of CHOEs, suggesting that South Asia has vulnerable climate regions due to its coexisting heavy stress of climate and population patterns, which was in line with a previous report.[46] It has been proposed that rapid population growth, high population density, inadequate infrastructure, and limited resources can jointly exacerbate the vulnerability to hazards in South Asia.[47] Overall, these findings have important implications that local policymakers should make targeted regional measurements based on heterogeneity in contributors of CHOEs and put more emphasis on the balance between increased population and resources when devising mitigation and adaption plans for health protection, especially in South Asia.[45]

To further distinguish the specific vulnerable regions for CHOEs, we explored the spatiotemporal variation and death burden among 218 countries/regions and screened out several hotspot cities or countries across the globe (Kuwait; the Arab Republic of Egypt; Macao, China; Bahrain; Qatar; Yemen; and India). It is unsurprising that most of these hotspots are coastal regions, which have proposed to have the greatest and fastest growing exposure to heatwaves.[18] Previous evidence showed that coastal regions are usually close to the ocean or large bodies of water, which can influence the regional climate by making it relatively milder and more humid than that in inland

https://doi.org/10.1021/acs.est.5c17533
Environ. Sci. Technol. 2026, 60, 8404−8414

regions.[48] Besides, the majority of hotspot regions were located in the coastal Middle East, which were frequently influenced by the advection of hot air masses from desert areas and the water vapor advection from warm water bodies that can induce prolonged high temperatures in summer.[49] As the co-occurrence of high temperature and humidity is more likely to trigger heatwaves, coastal regions tend to have higher vulnerability to CHOEs. It should be also noted that most of these regions are high-income regions, and their intensified heat island effects resulting from rapid urban development will make local people exposure to more pronounced heatwaves.[50] In addition, according to the estimate from the United Nations Environment Programme 2019, there were almost 38% of the global population living within 100 km of the coast, with a population density twice the global average.[51] The higher vulnerability of exposure and continuous aggregation of population coincide, making coastal regions rank in overall susceptibility to CHOEs.

While significant increasing trends of population exposure to CHOEs have been evident since 2000, they are not monotonic across time. Our study is the first to uncover that the temporal changes in population exposure to CHOEs are increasing at an accelerating pace in the presence of anthropogenic climate change. Lower-middle-income countries and South Asia showed the fastest increase in population exposure changes, with values nearly doubling in two decades (2021 vs 2002). Moreover, exposure effects contributed the most to population exposure changes in the majority of the globe; notably, population effect was another important contributor to population exposure changes in low-income countries and South Asia. A larger population means that more people will be exposed to climatic hazards. Besides, population growth is also related to a reduction in per capita income growth, which can directly cause an increase in poverty.[52] Overall, although coping with the increasing exposure is still a major action in future prevention and control for CHOEs, our finding provides important reminders that the growing populations (e.g., marginalized groups) and their collateral influence should be particularly regarded as a priority, especially in low-income countries.[53]

The key strength of this study is that we estimated CHOEs using meteorological and air pollutant data from relatively high spatial resolution data sets with a long period of two decades. In comparison with the only relevant study that used data with a spatial resolution of 1.25 ° × 1.875 °, our higher spatial resolution (0.1 ° × 0.1 °, nearly 120 times) allows us to provide a more precise estimate of CHOEs with the consideration of personal adaptations and identification of vulnerable regions. Besides, we employed the combination of multiple weather conditions to define heatwaves, which can accurately reflect people's perceived temperatures and provide more accurate assessments for population exposures.[54]

Our study also has certain limitations. Like other investigations that used satellite-derived data to identify exposures, the accuracy of our results directly depended on the quality of reanalysis data (i.e., uncertainties between observational and reanalysis data), which may raise concerns of under- or overestimation in our estimates. Although the predictive performances of ERA5-Land and GHAP were generally high on both global and regional scales, it is possibly insufficient to diagnose systematic biases in sparsely monitored regions and under extreme condition. Further research is warranted to evaluate the spatially stratified performance diagnostics to help provide more information on the likely direction and plausible magnitude of bias in our hotspot detection and burden estimates. Additionally, the definition of CHOEs was based on the distribution of temperatures and air quality guideline values without consideration of the potential health impacts of CHOEs, which may limit the generalization of our results. Due to the lack of data on the associations of exposure to CHOEs with mortality on a global scale and the daily or monthly mortality rates for each region, we employed risk estimates of exposure to heatwaves and O_3 separately from different worldwide studies to estimate the mortality risks and then combined them with yearly mortality rate to calculate the death burden attributable to CHOE exposure, which cannot consider the possible impact of certain within-country or within-year heterogeneity (e.g., urban-rural structure, health-care access, age composition, and death rate) and may introduce uncertainties in calculating PAF; thereby, it should be cautious when interpreting our results to other regions or populations. Furthermore, we did not evaluate the death burden of CHOEs in subpopulations (e.g., by sex or age) due to the lack of data on specific risk estimates. Future studies are warranted to estimate subpopulation-specific exposure-response associations of exposure to heatwaves, O_3 pollution, and CHOEs on a global scale, which can help provide deeper insights into the protection of vulnerable populations.

Our study provides novel evidence that the frequency, duration, and intensity of CHOEs and their population exposures displayed pronounced increasing trends and posed substantial death burdens both regionally and globally in the past nearly two decades. Midlatitude regions, particularly the Middle East and North Africa and South Asia, were CHOE hotspots. These findings have crucial implications in developing targeted mitigation strategies and prioritizing the acquisition and allocation of resources to reduce the health risks of CHOEs, especially for vulnerable hotspots.

■ ASSOCIATED CONTENT

Supporting Information

The Supporting Information is available free of charge at https://pubs.acs.org/doi/10.1021/acs.est.5c17533.

Spatiotemporal variation and death burden of compound heatwave and ozone pollution events (PDF)

■ AUTHOR INFORMATION

Corresponding Authors

Jing Wei − *MEEKL-AERM, College of Environmental Sciences and Engineering, Institute of Tibetan Plateau, and Center for Environment and Health, Peking University, Beijing 100871, China*; Email: jingwei@pku.edu.cn

Yuewei Liu − *Department of Epidemiology, School of Public Health, Sun Yat-sen University, Guangzhou 510080, China*; orcid.org/0000-0001-5970-4262; Email: liuyuewei@mail.sysu.edu.cn

Authors

Ruijun Xu − *Department of Epidemiology, School of Public Health, Sun Yat-sen University, Guangzhou 510080, China*

Yuxin Bi − *Department of Epidemiology, School of Public Health, Sun Yat-sen University, Guangzhou 510080, China*

Xiaohong Jia − *Department of Epidemiology, School of Public Health, Sun Yat-sen University, Guangzhou 510080, China*

https://doi.org/10.1021/acs.est.5c17533
Environ. Sci. Technol. 2026, 60, 8404−8414

Yi Zheng − *Department of Epidemiology, School of Public Health, Sun Yat-sen University, Guangzhou 510080, China*
Nongping Feng − *Department of Non-Communicable Disease Prevention and Control, Shenzhen Longgang Center for Chronic Disease Control, Shenzhen 518172, China*
Sirong Wang − *Department of Epidemiology, School of Public Health, Sun Yat-sen University, Guangzhou 510080, China*
Lu Luo − *Department of Epidemiology, School of Public Health, Sun Yat-sen University, Guangzhou 510080, China*
Ziquan Lv − *Central Laboratory of Shenzhen Center for Disease Control and Prevention, Shenzhen 518055, China*
Suli Huang − *School of Public Health, Shenzhen University Medical School, Shenzhen University, Shenzhen 518060, China;* orcid.org/0000-0003-3864-308X
Xue-Yan Zheng − *Institute of Non-Communicable Disease Control and Prevention, Guangdong Provincial Center for Disease Control and Prevention, Guangzhou 511430, China*
Hong Sun − *Department of Environment and Health, Jiangsu Provincial Center for Disease Control and Prevention, Nanjing 210009, China;* orcid.org/0000-0003-1467-6143
Gongbo Chen − *Climate, Air Quality Research Unit, School of Public Health and Preventive Medicine, Monash University, Melbourne, VIC 3004, Australia*

Complete contact information is available at: https://pubs.acs.org/10.1021/acs.est.5c17533

Author Contributions

○R.X. and Y.B. contributed equally to this work. Y.L. contributed to the study's conceptualization. R.X. and Y.B. contributed to the study methods. R.X. performed the formal analysis, wrote the original draft, and contributed to the visualization of all the figures and tables. Y.B., X.J., Y.Z., N.F., S.W., L.L., Z.L., X.Y.Z., S.H., H.S., and G.C. contributed to the review and editing of subsequent drafts. Y.L. and J.W. supervised all the data analysis and paper writing. The corresponding authors (Y.L. and J.W.) accessed and verified all the data in the study and had final responsibility for the decision to submit for publication after obtaining approval from all coauthors.

Notes

The authors declare no competing financial interest.

■ ACKNOWLEDGMENTS

This work was supported by the National Natural Science Foundation of China (grant 82574045), the Guangdong Basic and Applied Basic Research Foundation (grant 2025A1515011041), the Key Project of Medical Science Research of Jiangsu Provincial Health Commission (grant K2023045), and the Postdoctoral Fellowship Program of Chinese Postdoctoral Science Foundation (grant GZB20250194).

■ REFERENCES

(1) Domeisen, D.; Eltahir, E. A. B.; Fischer, E. M.; Knutti, R.; Perkins-Kirkpatrick, S. E.; Schar, C.; Seneviratne, S. I.; Weisheimer, A.; Wernli, H. Prediction and projection of heatwaves. *Nat. Rev. Earth Environ.* **2023**, *4* (1), 36−50.
(2) Intergovernmental Panel on Climate Change. Climate Change 2022: Impacts, Adaptation and Vulnerability. Cambridge University Press, 2022.
(3) World Economic Forum. Quantifying the Impact of Climate Change on Human Health. 2024.
(4) van Loenhout, J.; Below, R. Human cost of disasters: an overview of the last 20 years 2000−2019.*Centre for Research on the Epidemiology of Disasters United Nations Office for Disaster Risk Reduction* 2020.
(5) Pusede, S.; Steiner, A.; Cohen, R. Temperature and recent trends in the chemistry of continental surface ozone. *Chem. Rev.* **2015**, *115* (10), 3898−3918.
(6) Liang, S.; Chen, Y.; Sun, X.; Dong, X.; He, G.; Pu, Y.; Fan, J.; Zhong, X.; Chen, Z.; Lin, Z.; et al. Long-term exposure to ambient ozone and cardiovascular diseases: evidence from two national cohort studies in China. *J. Adv. Res.* **2024**, *62*, 165−173.
(7) Liu, W.; Hegglin, M. I.; Checa-Garcia, R.; Li, S.; Gillett, N. P.; Lyu, K.; Zhang, X.; Swart, N. C. Stratospheric ozone depletion and tropospheric ozone increases drive Southern Ocean interior warming. *Nat. Clim. Chang.* **2022**, *12* (4), 365−372.
(8) Lin, M.; Horowitz, L.; Xie, Y.; Paulot, F.; Malyshev, S.; Shevliakova, E.; Finco, A.; Gerosa, G.; Kubistin, D.; Pilegaard, K. Vegetation feedbacks during drought exacerbate ozone air pollution extremes in Europe. *Nat. Clim. Chang.* **2020**, *10* (8), 791.
(9) Schnell, J.; Prather, M. Co-occurrence of extremes in surface ozone, particulate matter, and temperature over eastern North America. *Proc. Natl. Acad. Sci. USA* **2017**, *114* (11), 2854−2859.
(10) Ban, J.; Lu, K.; Wang, Q.; Li, T. Climate change will amplify the inequitable exposure to compound heatwave and ozone pollution. *One Earth* **2022**, *5* (6), 677−686.
(11) Su, J.; Jiao, L.; Xu, G. Intensified exposure to compound extreme heat and ozone pollution in summer across Chinese cities. *npj Clim. Atmos. Sci.* **2025**, *8* (1), 78.
(12) Wang, C.; Hu, X. M.; Feron, S.; Leffel, J.; Cordero, R. R. Compound heat and ozone pollution in the urban environment. *Urban Clim.* **2025**, *62*, 102511.
(13) Analitis, A.; Michelozzi, P.; D'Ippoliti, D.; de'Donato, F.; Menne, B.; Matthies, F.; Atkinson, R. W.; Iñiguez, C.; Basagaña, X.; Schneider, A.; et al. Effects of heat waves on mortality. *Epidemiology* **2014**, *25* (1), 15−22.
(14) Du, H.; Yan, M.; Liu, X.; Zhong, Y.; Ban, J.; Lu, K.; Li, T. Exposure to concurrent heatwaves and ozone pollution and associations with mortality risk: a nationwide study in China. *Environ. Health Persp.* **2024**, *132* (4), 47012.
(15) Xu, R.; Sun, H.; Zhong, Z.; Zheng, Y.; Liu, T.; Li, Y.; Liu, L.; Luo, L.; Wang, S.; Lv, Z.; et al. Ozone, heat wave, and cardiovascular disease mortality: a population-based case-crossover study. *Environ. Sci. Technol.* **2024**, *58* (1), 171−181.
(16) Romanello, M.; McGushin, A.; Di Napoli, C.; Drummond, P.; Hughes, N.; Jamart, L.; Kennard, H.; Lampard, P.; Solano Rodriguez, B.; Arnell, N.; et al. The 2021 report of the Lancet Countdown on health and climate change: code red for a healthy future. *Lancet* **2021**, *398* (10311), 1619−1662.
(17) Muñoz-Sabater, J.; Dutra, E.; Agustí-Panareda, A.; Albergel, C.; Arduini, G.; Balsamo, G.; Boussetta, S.; Choulga, M.; Harrigan, S.; Hersbach, H.; et al. ERA5-Land: a state-of-the-art global reanalysis dataset for land applications. *Earth Syst. Sci. Data* **2021**, *13* (9), 4349−4383.
(18) Zhou, Y.; Gu, S.; Yang, H.; Li, Y.; Zhao, Y.; Li, Y.; Yang, Q. Spatiotemporal variation in heatwaves and elderly population exposure across China. *Sci. Total Environ.* **2024**, *917*, 170245.
(19) Bhattarai, S.; Bista, S.; Sharma, S.; White, L. D.; Amini, F.; Talchabhadel, R. Spatiotemporal characterization of heatwave exposure across historically vulnerable communities. *Sci. Rep.* **2024**, *14* (1), 20882.
(20) Wei, J.; Li, Z.; Yang, Z.; Liu, X.; Wang, J.; Li, K.; Lu, X.; Zhang, L.; Liao, H.; Guo, Y. et al. Decadal reversal of global surface ozone pollution. *Preprint (Version 1) Research Square*. December, *11*, **2025**, DOI: 10.21203/rs.3.rs-8336189/v1 (accessed 2026−2-25).
(21) Bright, E.; Coleman, P.; Dobson, J. LandScan: a global population database for estimating populations at risk. *Photogramm. Eng. Rem. S.* **2000**, *66*, 849−858.

(22) Hong, C.; Zhang, Q.; Zhang, Y.; Davis, S. J.; Tong, D.; Zheng, Y.; Liu, Z.; Guan, D.; He, K.; Schellnhuber, H. J. Impacts of climate change on future air quality and human health in China. *Proc. Natl. Acad. Sci. USA* **2019**, *116* (35), 17193−17200.
(23) Giani, P.; Castruccio, S.; Anav, A.; Howard, D.; Hu, W.; Crippa, P. Short-term and long-term health impacts of air pollution reductions from COVID-19 lockdowns in China and Europe: a modelling study. *Lancet Planet. Health* **2020**, *4* (10), E474−E482.
(24) Anderson, G.; Bell, M.; Peng, R. Methods to calculate the heat index as an exposure metric in environmental health research. *Environ. Health Persp.* **2013**, *121* (10), 1111−1119.
(25) Guo, Y.; Gasparrini, A.; Armstrong, B. G.; Tawatsupa, B.; Tobias, A.; Lavigne, E.; Coelho, M. D. Z. S.; Pan, X.; Kim, H.; Hashizume, M.; et al. Heat wave and mortality: a multicountry, multicommunity study. *Environ. Health Persp.* **2017**, *125* (8), 087006.
(26) Xu, R.; Huang, S.; Shi, C.; Wang, R.; Liu, T.; Li, Y.; Zheng, Y.; Lv, Z.; Wei, J.; Sun, H.; et al. Extreme temperature events, fine particulate matter, and myocardial infarction mortality. *Circulation* **2023**, *148* (4), 312−323.
(27) Perkins-Kirkpatrick, S.; Lewis, S. Increasing trends in regional heatwaves. *Nat. Commun.* **2020**, *11* (1), 3357.
(28) Wang, Y.; Zhao, N.; Yin, X.; Wu, C.; Chen, M.; Jiao, Y.; Yue, T. Global future population exposure to heatwaves. *Environ. Int.* **2023**, *178*, 108049.
(29) Kan, H. World Health Organization air quality guidelines 2021: implication for air pollution control and climate goal in China. *Chinese Med. J.* **2022**, *135* (5), 513−515.
(30) Zhao, Q.; Li, S.; Ye, T.; Wu, Y.; Gasparrini, A.; Tong, S.; Urban, A.; Vicedo-Cabrera, A. M.; Tobias, A.; Armstrong, B.; et al. Global, regional, and national burden of heatwave-related mortality from 1990 to 2019: a three-stage modelling study. *PLoS Med.* **2024**, *21* (5), No. e1004364.
(31) Vicedo-Cabrera, A. M.; Sera, F.; Liu, C.; Armstrong, B.; Milojevic, A.; Guo, Y.; Tong, S.; Lavigne, E.; Kysely, J.; Urban, A.; et al. Short term association between ozone and mortality: global two stage time series study in 406 locations in 20 countries. *BMJ* **2020**, *368*, m108.
(32) Orellano, P.; Reynoso, J.; Quaranta, N.; Bardach, A.; Ciapponi, A. Short-term exposure to particulate matter (PM_{10} and $PM_{2.5}$), nitrogen dioxide (NO_2), and ozone (O_3) and all-cause and cause-specific mortality: systematic review and meta-analysis. *Environ. Int.* **2020**, *142*, 105876.
(33) Moran, P. The interpretation of statistical maps. *J. Roy. Stat. Soc. B* **1948**, *10* (2), 243−251.
(34) Anselin, L. Local indicators of spatial association - LISA. *Geogr. Anal.* **1995**, *27* (2), 93−115.
(35) Benjamini, Y.; Hochberg, Y. Controlling the false discovery rate: a practical and powerful approach to multiple testing. *J. Roy. Stat. Soc. B* **1995**, *57* (1), 289−300.
(36) Sen, P. K. Estimates of the regression coefficient based on Kendall's Tau. *J. Am. Stat. Assoc.* **1968**, *63* (324), 1379−1389.
(37) Eastman, J.; Sangermano, F.; Ghimire, B.; Zhu, H.; Chen, H.; Neeti, N.; Cai, Y.; Machado, E.; Crema, S. Seasonal trend analysis of image time series. *Int. J. Remote Sens.* **2009**, *30* (10), 2721−2726.
(38) Jones, B.; O'Neill, B.; McDaniel, L.; McGinnis, S.; Mearns, L. O.; Tebaldi, C. Future population exposure to US heat extremes. *Nat. Clim. Chang.* **2015**, *5* (7), 652−655.
(39) Nishant, N.; Ji, F.; Guo, Y.; Herold, N.; Green, D.; Di Virgilio, G.; Beyer, K.; Riley, M. L.; Perkins-Kirkpatrick, S. Future population exposure to Australian heatwaves. *Environ. Res. Lett.* **2022**, *17* (6), 064030.
(40) Du, H.; Yan, M.; Liu, X.; Zhong, Y.; Ban, J.; Lu, K.; Li, T. Exposure to concurrent heatwaves and ozone pollution and associations with mortality risk: a nationwide study in China. *Environ. Health Persp.* **2024**, *132* (4), 047012.
(41) Qi, J.; Wang, Y.; Wang, L.; Cao, R.; Huang, J.; Li, G.; Yin, P. The modification effect of ozone pollution on the associations between heat wave and cardiovascular mortality. *Innovation Med.* **2023**, *1* (3), 100043.
(42) Hondula, D.; Rocklöv, J.; Sankoh, O. Past, present, and future climate at select INDEPTH member Health and Demographic Surveillance Systems in Africa and Asia. *Glob. Health Action* **2012**, *5*, 19083.
(43) Rocque, R.; Beaudoin, C.; Ndjaboue, R.; Cameron, L.; Poirier-Bergeron, L.; Poulin-Rheault, R. A.; Fallon, C.; Tricco, A. C.; Witteman, H. O. Health effects of climate change: an overview of systematic reviews. *BMJ Open* **2021**, *11* (6), No. e046333.
(44) Chevance, G.; Fresán, U.; Hekler, E.; Edmondson, D.; Lloyd, S. J.; Ballester, J.; Litt, J.; Cvijanovic, I.; Araújo-Soares, V.; Bernard, P. Thinking health-related behaviors in a climate change context: a narrative review. *Ann. Behav. Med.* **2023**, *57* (3), 193−204.
(45) Levy, B.; Sidel, V.; Patz, J. Climate change and collective violence. *Annu. Rev. Public Health* **2017**, *38*, 241−257.
(46) Kyaw, A.; Hamed, M.; Kamruzzaman, M.; Shahid, S. Spatiotemporal changes in population exposure to heat stress in South Asia. *Sustain. Cities Soc.* **2023**, *93*, 104544.
(47) Goyal, M.; Singh, S.; Jain, V. Heat waves characteristics intensification across Indian smart cities. *Sci. Rep.* **2023**, *13* (1), 14786.
(48) French, J.; Burningham, H. Coasts and climate: insights from geomorphology. *Prog. Phys. Geog.* **2013**, *37* (4), 550−561.
(49) Chen, X.; Li, N.; Liu, J.; Zhang, Z.; Liu, Y. Global heat wave hazard considering humidity effects during the 21st century. *Int. J. Environ. Res. Public Health* **2019**, *16* (9), 1513.
(50) Li, Y.; Schubert, S.; Kropp, J. P.; Rybski, D. On the influence of density and morphology on the Urban Heat Island intensity. *Nat. Commun.* **2020**, *11* (1), 2647.
(51) Lena, R.; Athanasios, T.; Lars, E. Population development as a driver of coastal risk: current trends and future pathways. *Cambridge Prisms: Coastal Futures* **2023**, *1*, No. e14.
(52) Dodson, J.; Dérer, P.; Cafaro, P.; Götmark, F. Population growth and climate change: addressing the overlooked threat multiplier. *Sci. Total Environ.* **2020**, *748*, 141346.
(53) Ratnam, J.; Owuor, M.; Greve, M.; Fu, C.; Stevens, N.; Mekuria, W.; Fidelis, A.; De Cauwer, V.; Lele, S.; Begotti, R. A.; et al. Trees as nature-based solutions: a global south perspective. *One Earth* **2020**, *3* (2), 140−144.
(54) Zhang, K.; Li, Y.; Schwartz, J. D.; O'Neill, M. S. What weather variables are important in predicting heat-related mortality? A new application of statistical learning methods. *Environ. Res.* **2014**, *132*, 350−359.

https://doi.org/10.1021/acs.est.5c17533
Environ. Sci. Technol. 2026, 60, 8404−8414